JOURNAL OF APPLIED PHYSICS **97**, 084503 (2005)

Transient thermal analysis of InGaAsP-InP high-power diode laser arrays with different fill factors

A. Gourevitch[a)]
State University of New York at Stony Brook, Stony Brook, New York 11794-2350

B. Laikhtman[b)] and D. Westerfeld
Power Photonic, Stony Brook, New York 11794-3717

D. Donetsky and G. Belenky
State University of New York at Stony Brook, Stony Brook, New York 11794-2350

C. W. Trussell
United States Army Nevada and Environment and Safety Directorate, 10215 Burbeck Rd., Ft. Belvoir, Virginia 22060-5806

Z. Shellenbarger, H. An, and R. U. Martinelli
Sarnoff Corporation, 201 Washington Rd., Princeton, New Jersey 08543

(Received 27 September 2004; accepted 8 February 2005; published online 1 April 2005)

The temperature kinetics of InGaAsP/InP high-power laser diode arrays with different fill factors was studied experimentally and theoretically. It was shown that except during a short initial period, the laser array heating is determined by the heat flux propagation through the heat spreader. To characterize this heating, we developed a two-dimensional analytical model. Experimentally, the temperature change in the active region was obtained by measuring the laser spectrum's temporal evolution during a single current pulse. Three distinctive periods in the transient heating process were clearly identified—an initial temperature rise, a square-root-of-time dependence of the active-region temperature increase, and an exponential approach of the active-region temperature to its steady-state value. We demonstrated that in the initial period of time, the heat propagates within the laser bar structure, and the laser bar design (fill factor) strongly affects the active-region temperature rise. In the later periods the temperature kinetics is insensitive to the fill factor. © *2005 American Institute of Physics*. [DOI: 10.1063/1.1884251]

I. INTRODUCTION

High wall-plug efficiency and a wide range of available wavelengths make laser diode arrays (LDA) preferable for many high-power applications, such as material processing, free-space communications, and especially for pumping of high-power solid-state lasers.[1–3] The high heat dissipation in the laser arrays makes effective thermal management a critical issue for reliable and efficient operation.

We have recently developed high-power laser arrays suitable for near-resonant pumping of erbium-doped solid-state lasers.[4] The optical pumping scheme requires high-power sources that can reliably provide a large fraction of their output energy in relatively narrow erbium absorption bands. The erbium fluorescence lifetime of about 5–10 ms favors relatively long pump-laser pulses.[5,6] The long current-injection pulses produce a considerable temperature increase within the diode laser structure that induces a redshift of the output wavelength. The thermal drift of the laser array emission spectra can lead to a misalignment with the erbium absorption bands. The pump-laser power falling outside these bands cannot be absorbed and is wasted, deteriorating the pumping efficiency.

The reliability of pumping arrays is another important issue for solid-state laser systems. Laser-array degradation mechanisms are enhanced by high operational temperatures, and aging tests indicate that the laser array lifetime decreases exponentially with the active-region temperature.[7]

Another key parameter for optically pumped solid-state laser systems is the output power of the pumping diodes, which is known to saturate with temperature. In recent years, many groups optimized the design of laser arrays to decrease the thermal load and to maximize the output power in different operating regimes.[1,8,9] It was shown that arrays with high emitter density (large fill factor) are preferred for short-pulse high peak power operation,[10,11] while arrays with low emitter density (small fill factor) are better suited for long-pulse, high average power operation.[12]

For efficient near-resonant pumping of erbium solid-state lasers, the design of the laser bars and the package architecture should minimize the active-region temperature rise, and hence, minimize the pump-laser spectral redshift throughout the long pulse duration. A comprehensive thermal analysis of the packaged laser arrays provides a powerful tool for design optimization. The steady-state temperature distributions in semiconductor laser diodes were evaluated from numerical[13] and analytical[14–16] solutions of the heat conductance equation with different boundary conditions. The transient thermal response of high-power LDAs was

[a)]Electronic mail: gourevitch@ece.sunysb.edu
[b)]Permanent address: Racah Institute of Physics, Hebrew University, Jerusalem, 91904, Israel.

TABLE I. InGaAsP/InP laser heterostructure.

Layer	Composition	Thickness (nm)
p-clad	InP:Zn	1500
Outer SCH	InGaAsP (1.13 eV)	300
Inner SCH	InGaAsP (1 eV)	30
Barrier (2)	InGaAsP (1 eV)	16
QW (3)	InGaAsP (0.8 eV) 1% of compressive strain	6
Inner SCH	InGaAsP (1 eV)	30
Outer SCH	InGaAsP (1.13 eV)	300
n-clad	InP:Se	1500

studied experimentally[17] and theoretically[18] for laser bars with planar heat spreaders. The current work reports on the effect of the laser bar design on the transient temperature change for laser bars mounted in bar-in-groove heat spreaders. We demonstrate the good agreement between the theoretical modeling and the experimental results. In Sec. II, the laser bar design and the heating kinetics measurements are discussed. A description of the theoretical model is presented in Sec. III. Section IV discusses the experimental results and their comparison with the analytical model.

II. DEVICE STRUCTURE AND HEATING KINETICS MEASUREMENTS

The InGaAsP/InP laser structure emitting at 1.5 μm was grown by metalloorganic chemical vapor deposition. The active region contains three 6-nm InGaAsP quantum wells (QWs) with 1% compressive strain separated by 16-nm InGaAsP barriers. A double-step graded-index separate confinement heterostructure (SCH) with 300-nm-thick outer and 30-nm-thick inner InGaAsP layers provides optical confinement. The broadened waveguide (710 nm) was incorporated between *n*- and *p*-clad layers, each 1.5-μm thick. The *n*-cladding was doped with Se with a concentration of 5×10^{17} cm^{-3} and the *p*-cladding was gradually doped with Zn with an average concentration of 7.5×10^{17} cm^{-3}. All layers, the composition and thickness of which are given in Table I, except the QWs were grown lattice-matched to the InP substrate. The total thickness of the laser bar structure including the substrate was 140 μm. The 100-μm-wide, 1-mm-long laser stripes were equally spaced along the 1-cm-wide laser bar and were separated by unpumped regions. The laser bars with 10%, 20%, and 40% fill factors (FF) were fabricated, where FF is the ratio of the pumped area to the total laser bar area. These bars were mounted onto metallized grooves in 2-mm-thick BeO heat spreaders bonded to water-cooled microchannel heat sinks; see the inset of Fig. 1(a). Details of the laser heterostructure and bar design were reported elsewhere.[4,19] The laser diode arrays with different FFs showed a threshold current density of 480 A/cm^2 and a slope efficiency of 0.5 W/A in the linear part of the light-current characteristic at room temperature.

The temperature kinetics in the active region was determined by measuring the temporal evolution of the laser spectra during a 400-ms current pulse. The pulse duration was chosen to be long enough to reach a steady-state operation

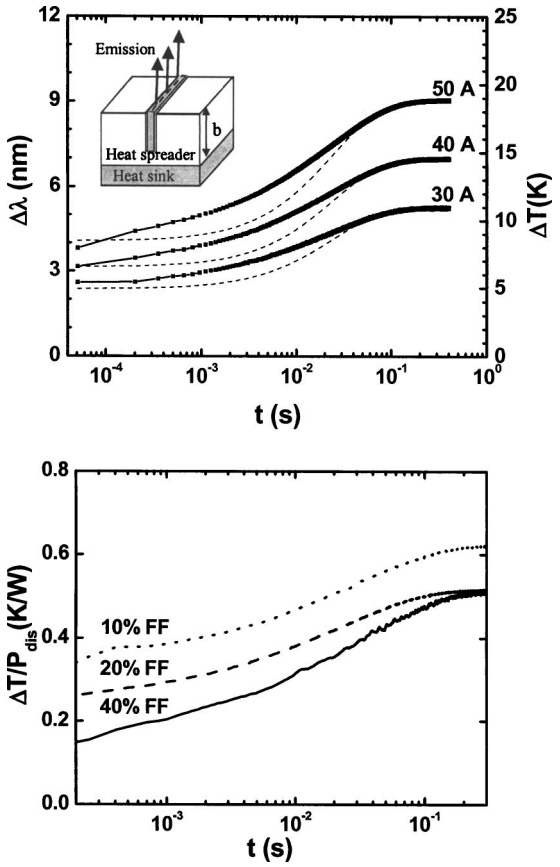

FIG. 1. (a) Time dependence of the average wavelength shift (left axis) and the corresponding active-region temperature change (right axis) for a 1.5 -μm laser diode array with 20% fill factor. The result of the analytical calculation of the average thermal kinetics is shown by dashed lines for 30-, 40-, and 50-A drive currents. (b) Active-region temperature rise divided by dissipated power (i.e., thermal resistance) as a function of time for 10%, 20%, and 40% FF arrays.

regime. The spectrum evolution was measured using a 0.5 -m grating monochromator equipped with a linear 256-pixel InGaAs photodetector. The photodetector array captured the laser array spectrum with a resolution of 0.16 nm without rotating the diffraction grating. The total full-width at half-maximum (FWHM) spectral width for the arrays was typically around 10–15 nm, while single emitters cleaved from the same wafer exhibit a typical FWHM spectral width of 5 nm. The coupling of the laser emission into the monochromator was performed using an integrating sphere. The emission spectra was recorded every 100 μs during the current pulse. Recording all the spectra during a single current pulse ensured highly accurate measurements. For a quantitative characterization of the spectrum redshift with time during the current pulse, we computed the weighted average[17] wavelength of each emission spectrum and subtracted the weighted average wavelength of the emission spectrum measured at the beginning of the pulse.

Figure 1(a) shows the weighted average wavelength shift and the average active-region temperature change for the 20% FF array at drive currents of 30, 40, and 50 A. A conversion coefficient between the wavelength shift and the active-region temperature was obtained by measuring the laser spectral shift under low-duty cycle (0.02%), short-pulse

(200 ns) operation at a variety of heat sink temperatures. The heating kinetics was measured for arrays with 10%, 20%, and 40% FF over a wide range of total dissipated power. Figure 1(b) shows the temperature change divided by the bar dissipated power for arrays with different FFs. The total dissipated power P_{dis} equals the difference between the input electrical power and the output optical power. The data show that the active-region temperatures (for the same dissipated power) in arrays with 10%, 20%, and 40% FF are significantly different during the first few hundred microseconds. The temperature difference between the 20% and 40% FF arrays diminishes over time, while the 10% FF array demonstrates higher temperatures for all times. This steady-state thermal behavior correlates the thermal resistances of the arrays determined in Ref. 4.

III. THEORY

A. Model

To describe the transient active-region thermal behavior of laser arrays, we developed an analytical model including the main features of the laser array assembly. The schematic cross section of the array assembly considered in the model is shown in Fig. 2. The BeO heat spreader occupies the region $0<y<b$ and isothermally contacts an ideal heat sink at $y=b$. The bottom edge ($y=0$) of the heat spreader is adiabatically isolated. The thickness of the heat spreader is at least one order of magnitude larger than the thickness of the laser bar. Because of this, we neglect the thickness of the laser bar, which can be represented by a homogeneous heat source located at $x=0$, $0<y<a$ and shown in Fig. 2 by the line *AB*. The heat conductance problem is reduced to the solution of the equation

$$\frac{\partial \Delta T}{\partial t}=\chi\left(\frac{\partial^2 \Delta T}{\partial x^2}+\frac{\partial^2 \Delta T}{\partial y^2}\right) \tag{1}$$

with the following boundary conditions:

$$\Delta T|_{y=b}=0, \qquad \kappa\frac{\partial \Delta T}{\partial y}\bigg|_{y=0}=0,$$
$$\kappa\frac{\partial \Delta T}{\partial x}\bigg|_{x=0}=-Q\theta(a-y), \tag{2}$$

where ΔT is the temperature change due to heating, χ and κ are the BeO thermal diffusivity and conductivity, respectively, and Q is the heat flux density from the laser structure. Due to the symmetry of the problem, we consider only the region $x>0$. The equation is solved using the Laplace transformation, and the result is

$$\Delta T(x,y,t)=\frac{4Q\sqrt{\chi}}{\pi\kappa}\sum_{n=0}^{\infty}\frac{1}{2n+1}\sin\left[\frac{\pi(2n+1)a}{2b}\right]\cos\left[\frac{\pi(2n+1)y}{2b}\right]\frac{1}{2\pi i}\int_{\delta-i\infty}^{\delta+i\infty}\frac{\exp[pt-x\sqrt{p+(2n+1)^2/\tau}/\sqrt{\chi}]}{p\sqrt{p+(2n+1)^2/\tau}}dp, \tag{3}$$

where $\tau=4b^2/\pi^2\chi$ is the relaxation time. The contour integral can be reduced to a definite one with the help of the expansion in poles of the integrand,

$$\Delta T(x,y,t)=\Delta T_0(x,y)-\frac{16Qb}{\pi^3\kappa}\sum_{n=0}^{\infty}\frac{1}{2n+1}e^{-(2n+1)^2t/\tau}\sin\left[\frac{(2n+1)\pi a}{2b}\right]\cos\left[\frac{(2n+1)\pi y}{2b}\right]\int_0^{\infty}e^{-r^2t/\tau}\left[\frac{\cos(\pi r^2x/2b)}{r^2+(2n+1)^2}\right]dr, \tag{4}$$

where

$$\Delta T_0(x,y)=\frac{8Qb}{\pi^2\kappa}\sum_{n=0}^{\infty}\frac{1}{(2n+1)^2}e^{-\pi(2n+1)x/2b}\sin\left[\frac{(2n+1)\pi a}{2b}\right]\cos\left[\frac{(2n+1)\pi y}{2b}\right] \tag{5}$$

is the steady-state temperature.

For comparison with our experimental results, we computed the average temperature change. The temperature averaged over the stripe was defined as

$$\Delta\overline{T}(t)\equiv\frac{1}{a}\int_0^a\Delta T(0,y,t)dy. \tag{6}$$

In the comparison of our theoretical calculation with the experimental results we were interested mainly on the functional dependence of the temperature on time and not on the absolute value of the temperature, which is dependent on physical parameters known with some uncertainty. As such, we treated the prefactor [$16\ Qb/\pi^3\kappa$ in Eq. (4)] as an adjustable parameter chosen to fit the computed results at large time to the experimentally determined steady-state temperature rise.

B. Three heating periods

The real geometry is more complicated than the geometry considered in the theoretical model due to the finite thickness of the laser bar, a nonuniform heat source distribution in the bar, and the nonideality of the water-cooled heat sink. The first two factors are important in the short-time scale and the last one affects the estimation of the relaxation time τ, which describes longer-time-scale heating. The heating of the laser bar structure controls the initial active-region

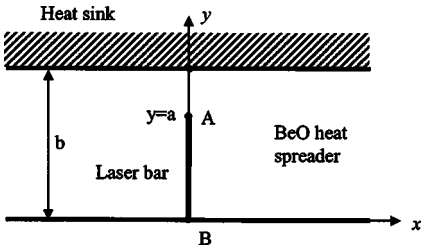

FIG. 2. The cross section geometry of the laser array assembly used for the calculation of the temperature distribution is shown. The BeO heat spreader occupies the region $0<y<b$. The laser bar is plotted by the line *A*-*B*. The interface between the BeO heat spreader and the heat sink lies at $y=b$.

temperature rise. The heat is generated in the active regions under the metal stripe contacts and produces heat fluxes. The propagation of heat fluxes from the InP-based laser bar structure to the BeO heat spreader is hindered by the In-based solder layer serving as interface between these materials and the smaller value of thermal diffusivity of InP ($\chi_1 = 0.37$ cm^2/s) in comparison with BeO ($\chi = 0.9$ cm^2/s). During the initial period of heating, lateral heat spreading and heating of the laser bar occurs. The duration of this period τ_1 can be estimated as ℓ_1^2/χ_1, where $\ell_1 \sim 100$ μm is a characteristic length on the order of the thickness of the laser bars and the separation between adjacent stripes in the laser bar. The estimated value of τ_1 is about 100 μs. The initial heating of the laser bar structure was included in our model by assuming that the measurement starts with time delay $t_0 \approx \tau_1$ after the beginning of the current pulse. The analytically calculated heating kinetics is shown by the dashed lines in Fig. 1(a) for the 30-, 40-, and 50-A drive currents.

The analytical model describes the heating at $t > \tau_1$ after the entire laser bar has been heated and the nonuniformity of the heat source distribution is diminished. In this time range ($t > \tau_1$) it is possible to separate two periods when the temperature kinetics given by Eq. (4) can be greatly simplified. In the short-time kinetics $t \ll \tau$, i.e., the second period of heating, a simplified form of the solution can be obtained directly from Eqs. (3) and (6), where the condition $t \ll \tau$ corresponds to $p\tau \gg 1$. This gives

$$\Delta\overline{T}(t) = \frac{2Q\sqrt{\chi t}}{\kappa\sqrt{\pi}}. \tag{7}$$

The third period of heating is the long-time kinetics when $t \gg \tau$. In this period, the rapid decay of the exponential terms make it possible to approximate the temperature change using just one term ($n=0$) from the sum obtained by substituting Eq. (4) into Eq. (6).

$$\Delta\overline{T}(t) = \Delta\overline{T}_0\left(1 - \sqrt{\frac{\tau}{\pi t}}e^{-t/\tau}\right), \tag{8}$$

$$\text{where } \Delta\overline{T}_0 = \frac{8bQ}{\pi^2\kappa}\frac{2b}{\pi a}\sin^2\left(\frac{\pi a}{2b}\right).$$

In summary, the heating process can be subdivided into three time periods, each with different heat transport conditions. During the first period, the active-region temperature increase of laser arrays is determined by heating the structure very close to the laser stripes. As the first period progresses, the heat fluxes from individual laser stripes overlap, producing a nearly uniform heat flux. In the second period the unified heat flux propagates through the BeO heat spreader toward the cooler, but the substantially heated region is still much smaller than the thickness of the heat spreader. The heating kinetics is determined by Eq. (7) and the temperature change of the active region is proportional to the square-root of time. In the third period the heat flux has reached the heatsink, the entire BeO heat spreader is heated, and the active-region temperature asymptotically approaches its steady-state value, Eq. (8).

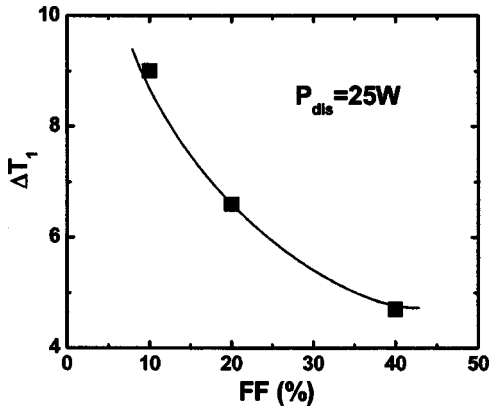

FIG. 3. Active-region initial temperature rise during the first 200 μs for 10%, 20%, and 40% FF arrays at a constant total bar P_{dis} of 25 W.

IV. RESULTS AND DISCUSSION

To study the initial heating ($t \leqslant \tau_1$) of laser arrays with different fill factors, the active-region temperature rise (ΔT_1) was measured for the first 200 μs. Figure 3 demonstrates the dependence of ΔT_1 on FF at 25-W total dissipated power per bar. The experimental results show that the temperature rise during the first 200 μs is highest for the array with a 10% FF and smallest for the array with 40% FF. In the first heating period the active-region heating is mainly determined by the power dissipation in each stripe. The dissipated power per stripe scales with the number of stripes for a constant total dissipated power in the bars. At a given dissipated power in the bar, the temperature rise decreases with the fill factor. This decrease is not directly proportional to the number of stripes. During the first 200 μs, the active-region temperature increases are 9 K for 10% FF, 6.5 K for 20% FF, and 4.5 K for 40% FF at 25-W dissipated power per bar. This is an evidence of the lateral heat transport in the laser bar structure that is responsible for the mutual heating of the adjacent emitters. This lateral heat transport leads to an overlapping of heat fluxes from the active-region areas under the metal contacts and to the homogenization of the temperature distribution in the laser bar.

The second period lasts while $\tau_1 < t \ll \tau$ and ends before the heat flux reaches the heat sink. Since in the first period the heat fluxes from under the stripe areas have merged into a nearly uniform flux, the thermal kinetics is expected to be independent of the distance between emitters (i.e., fill factor) in this second phase of heating. To analyze the active-region

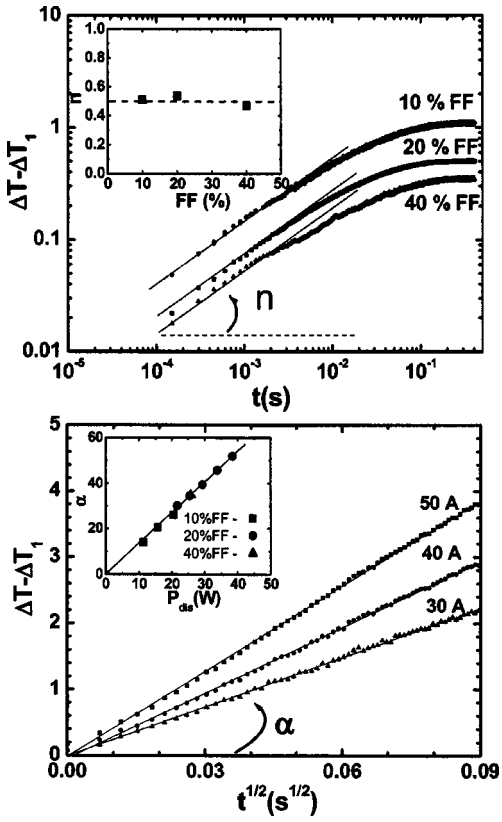

FIG. 4. (a) The temperature changes are plotted on double-log axes for the three fill factors. The solid lines were fitted to the experimental data over the time interval of 200 μs to 10 ms. The computed slopes are shown in the inset as a function of the fill factor. (b) The active-region temperature change of a 20% fill factor array is plotted vs the square-root of time with 30-, 40-, and 50-A drive currents at a coolant temperature of 18 °C. The dependency of the slope coefficient α on the total dissipated power is shown for 10% (square symbol), 20% (circle symbol), and 40% (triangle symbol) fill factor arrays in the inset.

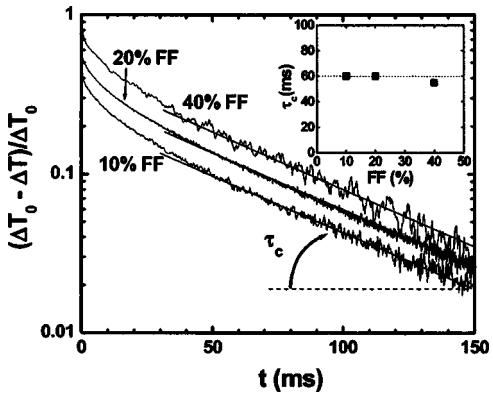

FIG. 5. Normalized deviation from steady-state temperature vs time is plotted for arrays with 10%, 20%, and 40% FF. The slopes of the solid lines are used to calculate τ_c, which is shown in the inset.

temperature change during the second period, the initial temperature rise (ΔT_1) was subtracted from the measured active-region temperature. Figure 4(a) shows the temperature change on double-log axes for arrays with the three different fill factors. The solid lines in Fig. 4(a) were fitted to the experimental data over the time interval from 200 μs to about 10 ms. The inset shows the computed slopes as a function of the fill factor. The slope of these fit lines is close to 0.5, indicating that the active-region temperature change increases as the square-root of time. Figure 4(b) shows the active-region temperature change versus the square-root of time for a 20% fill factor array at 30-, 40-, and 50-A drive currents, which corresponds to 21.5-, 29-, and 38.5-W total dissipated power. The temperature dependencies are well approximated by straight lines with the slope coefficient α. The measured slope coefficients have been plotted in the inset for 10%, 20%, and 40% FF arrays as functions of the total dissipated power. The slope coefficient increases linearly with the total dissipated power at the same rate for all three arrays. This shows that over the time scale $\tau_1 < t \ll \tau$ the temperature kinetics is determined by the free propagation of the nearly uniform heat flux in the BeO heat spreader and does not depend on the fill factor. This thermal behavior is well described by the asymptotic analytical solution of Eq. (7).

In the third period ($t \gg \tau$), the active-region temperature change approaches the steady-state value (ΔT_0) with a characteristic time constant τ and is characterized by long-time asymptotic kinetics given by Eq. (8). Equation (8) can be rewritten as

$$\frac{[\Delta T_0 - \Delta T(t)]}{\Delta T_0} = \sqrt{\frac{\tau}{\pi t}} \exp(-t/\tau). \tag{9}$$

For $t \gg \tau$, the exponential time dependence dominates the preceding term $\sqrt{\tau/\pi t}$, and Eq. (9) can be simplified as

$$\frac{[\Delta T_0 - \Delta T(t)]}{\Delta T_0} \sim \exp(-t/\tau). \tag{10}$$

In Fig. 5 the normalized difference between the active-region temperature change and the experimentally determined steady-state temperature rise (ΔT_0) is plotted in semilogarithmic scale for all three arrays. Figure 5 shows that for long times, $t > 20$ ms, the data are well approximated by the exponential time dependence given by Eq. (10) . The slopes of the solid lines in Fig. 5 were fitted to the data to calculate the experimental time constant τ_c, which is shown in the inset as a function of FF. The long-time heating kinetics of these arrays with different FFs can be characterized with the same τ_c of about 60 ms. The experimental time constant τ_c is larger than the theoretically calculated time constant, $\tau \approx 20$ ms. The reason for the discrepancy is that the theoretical model describes only the heat propagation through the heat spreader, while in reality there are other factors affecting the temperature kinetics, such as the nonideality of the water-cooled heat sink and the interface between the BeO heat spreader and the heat sink.

V. CONCLUSIONS

In conclusion, we report on the experimental and theoretical study of heating kinetics for InGaAsP/InP arrays with 10%, 20%, and 40% fill factors. The transient heating process can be divided into three time periods; each period is determined by its own heat transport condition. During the first period, the bar structure is heated and the heat fluxes from individual stripes of the laser bar overlap, producing the nearly uniform heat flux. The duration of this period (τ_1)

is determined by the geometry of the laser bar and its thermal diffusivity. The second period is characterized by the propagation of the nearly uniform heat flux through the BeO heat spreader. The heat propagation length for the second period is much smaller than the heat spreader thickness. By the third period the heat flux has reached the heat sink, the entire heat spreader has been heated, and the temperature distribution approaches the steady state.

The theoretical model describes the heating in the second and the third heating periods. In the second period the active-region temperature change of laser arrays is proportional to the square-root of time, and in the third period the deviation of the temperature from its steady-state value decreases exponentially with time. The initial temperature rise is included in the model by assuming a time delay $t_0 \approx \tau_1$ to heat the laser bar structure.

The temperature rise measured for the first 200 μs is dependent on the power dissipated per stripe and the distance between stripes. This initial temperature change decreases with the fill factor for a given total bar power dissipation and bar size. The second and third periods are well described by the asymptotic solutions of the theoretical model. The maximal difference between the analytically predicted temperature and the experimental one is about two degrees for the largest current, 50 A. This small difference indicates that our model adequately describes the array heating process. The discrepancy between the theoretical and experimental values of the time constant τ in the third heating period shows that the thermal properties of the interfaces and the nonideality of the heat sink substantially affect the heat flow.

ACKNOWLEDGMENTS

We would like to acknowledge the support of the present work from the Army Research Office, Grant No. ARO DAAD190310259, and the United States Air Force Office of Scientific Research, Grant No. F-49620-01-10108. One of us (B. L.) acknowledges the support of the Israel Science Foundation founded by the Israel Academy of Sciences and Humanities.

[1] J. G. Endriz *et al.*, IEEE J. Quantum Electron. **28**, 952 (1992).
[2] D. Botez and D. R. Scifres, *Diode Laser Arrays* (Cambridge University Press, Cambridge, 1994).
[3] G. Erbert, A. Barwolff, J. Sebastian, and J. Tomm, Top. Appl. Phys. **78**, 173 (2000).
[4] A. Gourevitch, G. Belenky, D. Donetsky, B. Laikhtman, D. Westerfeld, C. W. Trussell, H. An, Z. Shellenbarger, and R. Martinelli, Appl. Phys. Lett. **83**, 617 (2003).
[5] S. D. Setzler, P. A. Budni, and E. P. Chicklis, in *Advanced Solid-State Lasers*, OSA Trends in Optics and Photonics Vol. 50, edited by Christopher Marshall (Optical Society of America, Washington, DC, 2001), p. 309.
[6] S. D. Setzler, K. J. Snell, T. M. Pollak, P. A. Budni, Y. E. Young, and E. P. Chicklis, Opt. Lett. **28**, 1787 (2003).
[7] M. Fukuda, *Reliability and Degradation of Semiconductor Lasers and LEDs* (Artech House, Boston, 1991).
[8] S. A. Payne *et al.*, IEEE J. Sel. Top. Quantum Electron. **3**, 71 (1997).
[9] R. Beach, W. J. Benett, B. L. Freitas, D. Mundinger, B. J. Comaskey, R. W. Solarz, and A. Emanuel, IEEE J. Quantum Electron. **28**, 966 (1992).
[10] H. Q. Le, G. W. Turner, and J. R. Ochoa, IEEE Photonics Technol. Lett. **10**, 663 (1998).
[11] J. A. Skidmore, B. L. Freitas, C. E. Reinhardt, E. J. Utterback, R. H. Page, and M. A. Emanuel, IEEE Photonics Technol. Lett. **9**, 1334 (1997).
[12] M. Maiorov, R. Menna, V. Khalfin, H. Milgazo, R. Matarese, D. Garbuzov, and J. Connolly, IEEE Photonics Technol. Lett. **11**, 961 (1999); M. Maiorov, R. Menna, V. Khalfin, H. Milgazo, A. Triano, D. Garbuzov, and J. Connolly, Electron. Lett. **35**, 636 (1999).
[13] A. Barwolff, R. Puchert, P. Enders, U. Menzel, and D. Ackermann, J. Therm. Anal. **45**, 417 (1995).
[14] W. B. Joyce and R. W. Dixon, J. Appl. Phys. **14**, 1981 (1975).
[15] M. Ito and T. Kimuro, IEEE J. Quantum Electron. **17**, 787 (1981).
[16] B. Laikhtman, A. Gourevitch, D. Donetsky, D. Westerfeld, and G. Belenky, J. Appl. Phys. **95**, 3880 (2004).
[17] M. Voss, C. Lier, U. Menzel, A. Barwolff, and T. Elsaesser, J. Appl. Phys. **79**, 1170 (1996).
[18] R. Puchert, A. Barwolff, M. Voss, U. Menzel, J. W. Tomm, and J. Luft, IEEE Trans. Compon., Packag. Manuf. Technol., Part A **23**, 95 (2000).
[19] D. Z. Garbuzov, R. J. Menna, R. U. Martinelli, J. H. Abeles, and J. C. Connolly, Electron. Lett. **33**, 1635 (1997).